Angewandte Chemie
Eine Zeitschrift der Gesellschaft Deutscher Chemiker

Supporting Information

Selective Electrochemical Reduction of Carbon Dioxide to Ethanol on a Boron- and Nitrogen-Co-doped Nanodiamond

Yanming Liu[+], Yujing Zhang[+], Kai Cheng, Xie Quan, Xinfei Fan, Yan Su, Shuo Chen, Huimin Zhao, Yaobin Zhang, Hongtao Yu, and Michael R. Hoffmann*

anie_201706311_sm_miscellaneous_information.pdf

Table of Contents in Supporting Information

1. Experimental Methods

Preparation of BND, BDD and NDD electrodes. The BND, BDD and NDD electrodes were prepared by hot filament chemical vapor deposition method using Si as substrates. The Si wafer, n-Si (100) with resistivity of 0.001~0.005 Ω•cm, was ultrasonically washed by ethanol and ultrapure water for 10 minutes, respectively, and then immersed in oxidizing solution consisting of H_2SO_4 (97%) and H_2O_2 (35%) in a volume ratio 3:1 for 10 minutes to remove organics on its surface. After etching of the substrate in 10% HF solution for 5 minutes to remove the SiO_2 film, the Si substrate was ultrasonically pre-treated in a nanodiamond suspension (acetone as solvent) to polish the substrate surface and enhance BND nucleation density. Subsequently, BND films were grown on the pre-treated Si substrate at substrate temperature 600 ºC and pressure 500 Pa with a gas mixture of $CH_4/B_2H_6/N_2/H_2$ (2.5% CH_4). Three BND electrodes with B_2H_6 content of 12.5% and N_2 contents of 2.5%, 5.0% and 10.0% were prepared. As comparison, BDD with 12.5% B_2H_6 and NDD with 5.0% N_2 were also prepared under the same conditions.

Electrochemical experiments. All the electrochemical tests were performed in a three-electrode system at room temperature and pressure. BND, BDD or NDD was used as working electrode, Ag/AgCl and Pt foil were used as the reference electrode and counter electrode, respectively. Linear sweep voltammograms of BND electrodes for CO_2 reduction were collected at Ar or CO_2 saturated 0.1 M $NaHCO_3$ solution (scan rate of 100 mV s^{-1}). Electrochemical reduction of CO_2 was carried out in CO_2 saturated 0.1 M $NaHCO_3$ solution with a gas-tight H-type two-compartment cell (100 mL) separated by Nafion 117 membrane. It was conducted potentiostatically at -0.8 V~-1.2 V (vs RHE) with the cathode compartment continuously flushed with CO_2 gas. All potentials were quoted with respect to reversible hydrogen electrode (RHE), which were converted using the equation of $E_{vs\ RHE} = E_{vs\ Ag/AgCl} + 0.059 \times pH + 0.2$ (V). The area of each working electrode (BND, BDD or NDD) was 2 cm × 3 cm. The gaseous products were analyzed by gas chromatography (Shimadzu, GC-14C) equipped with a thermal conductivity detector (TCD). For the liquid product, ionized products such as $HCOO^-$ and CH_3COO^- were quantified by ion chromatography (Shimadzu SCL-10ASP); nonionic products such as

CH_3CH_2OH, CH_3OH and HCHO were analyzed by gas chromatography (Shimadzu, GC-2010) with flame ionization detector (FID).

Density functional theory computation. All calculations were carried out using the Vienna ab initio Simulation Package (VASP) based on density functional theory (DFT). A plane-wave basis was used with kinetic-energy cutoff of 450 eV. The Perdew-Burke-Ernzerhof (PBE) functional within generalized gradient approximation (GGA) was selected to treat the exchange-correlation interaction of electrons. The electron-ion interactions were described by the projector augmented wave (PAW) potentials. Γ-centered grids for Brillouin zone (BZ) integrations was applied with a uniform spacing of $2\pi \times 0.02$ $Å^{-1}$. To take into account the long-range van der Waals (vdW) interactions, the semi-empirical dispersion-corrected DFT-D3 scheme proposed by Grimme was adopted. The reaction pathway and energy barrier were calculated by climbing-image nudged elastic band (CI-NEB) method. Supercells of (4×4) diamond (111) surface and (4×3) diamond (220) surface were used for all simulations. To avoid the mirror effect between diamond surface and the periodically images, a vacuum space of 14 Å was inserted. All the optimization of small molecule is performed in a 20 Å simple cubic lattice and samples k points only at the Γ point. A convergence criterion of 1×10^{-4} eV for the total energies and 0.02 eV/Å for force were adopted. The adsorption energy of adsorbates was calculated from the equation $E_{ads}=E_{tot} - E_{dia} - E_{mol}$, where E_{tot}, E_{dia} and E_{mol} represent the total energy of the complex of diamond surface and adsorbates, diamond surface, and adsorbates, respectively.

2. Supplementary Figures

During BND preparation, carbon species nucleate on Si substrate to form nanodiamond crystal with growth direction of (111), (220) and (311). Meanwhile, B and N atoms are doped into nanodiamond crystal. As BND1, BND2 and BND3 were prepared using the same nanodiamond pretreated Si substrate under the same temperature, pressure, CH_4 and B_2H_6 contents but gradually increased N_2 content, the main facet changed from (111) for BND1 to (220) for BND2 and BND3 could be attributed to the increased N content. BND with low N content (BND1) is dominated by (111) facet. When its N content increased to some extent (BND2, BND3), twin crystals start to appear on the grain boundary and nanodiamond crystal preferentially grow in the (220) direction. The weaker peak intensity of BND3 relative to BND2 can be explained by the decreased diamond quality of BND3 (revealed by Raman spectra) due to heavy N doping.

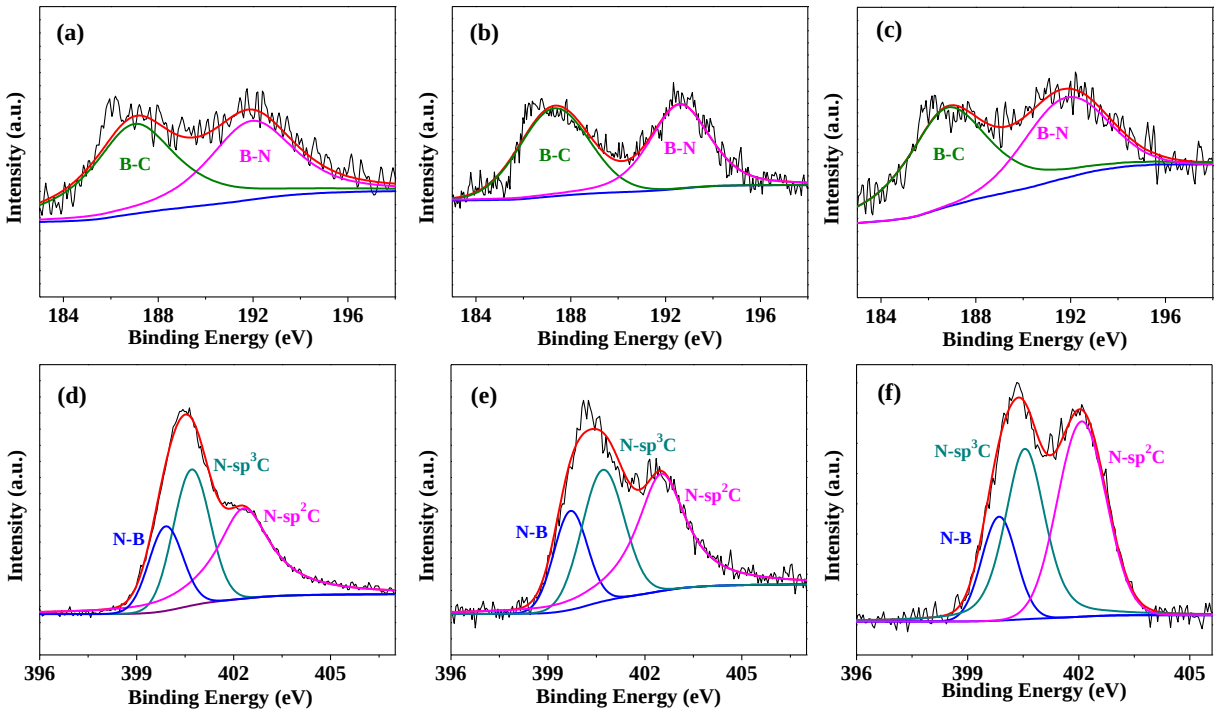

Figure S1. The B 1s XPS spectra of (a) BND1, (b) BND2 and (c) BND3, and N 1s XPS spectra of (d) BND1, (e) BND2 and (f) BND3.

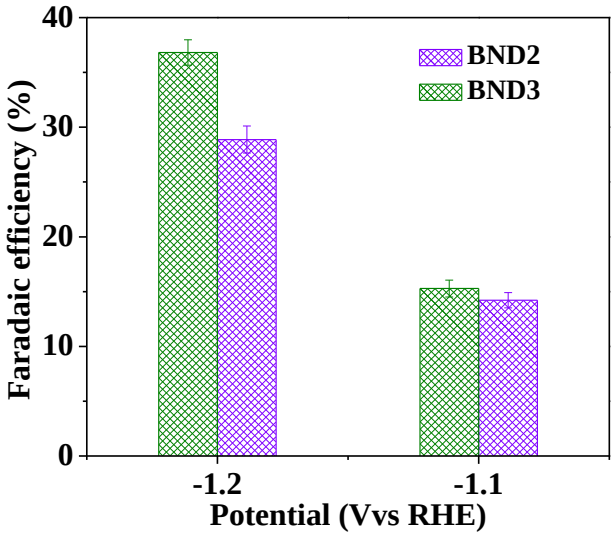

Figure S2. Faradaic efficiency for H_2 production on BND2 and BND3 electrodes at -1.1~-1.2 V.

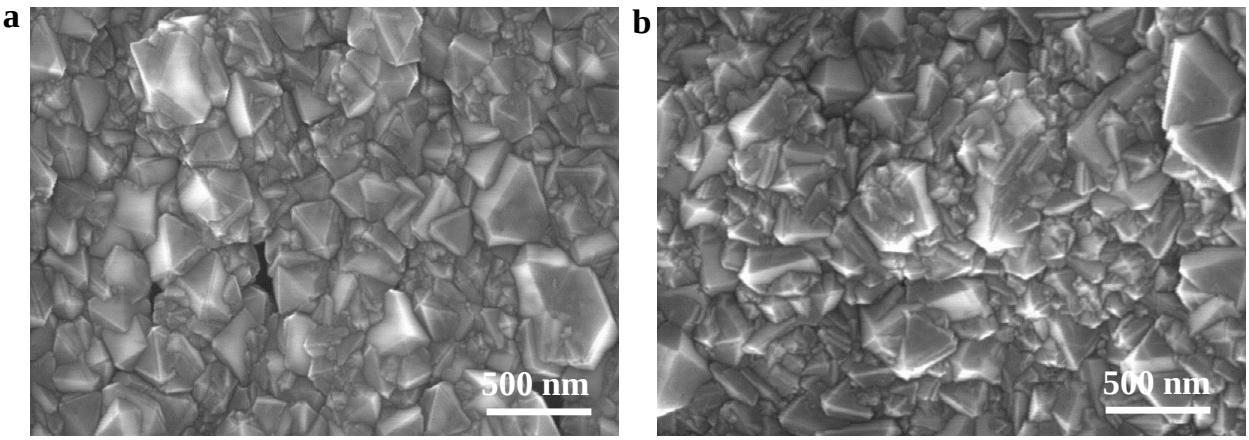

Figure S3. SEM images of (a) BDD and (b) NDD.

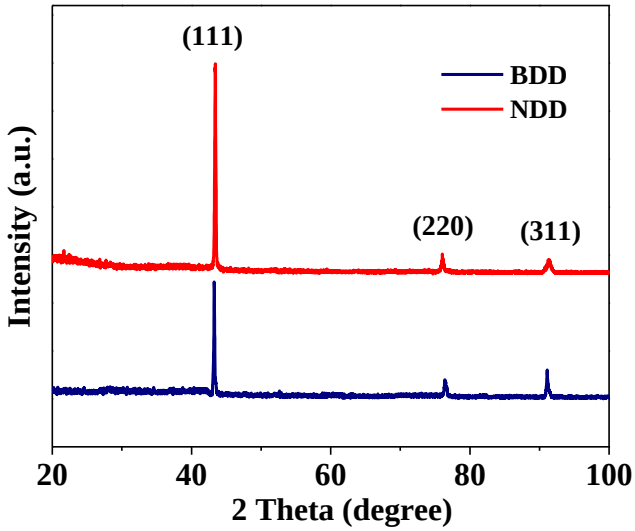

Figure S4. The XRD spectrums of BDD and NDD.

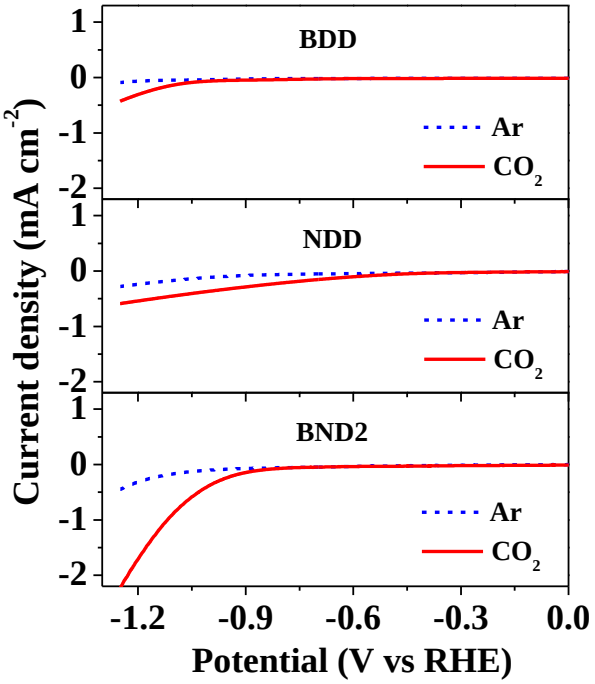

Figure S5. Linear sweep voltammograms of BDD, NDD and BND2 in Ar or CO_2 saturated 0.1 M $NaHCO_3$ solution (scan rate 100 mV s^{-1}).

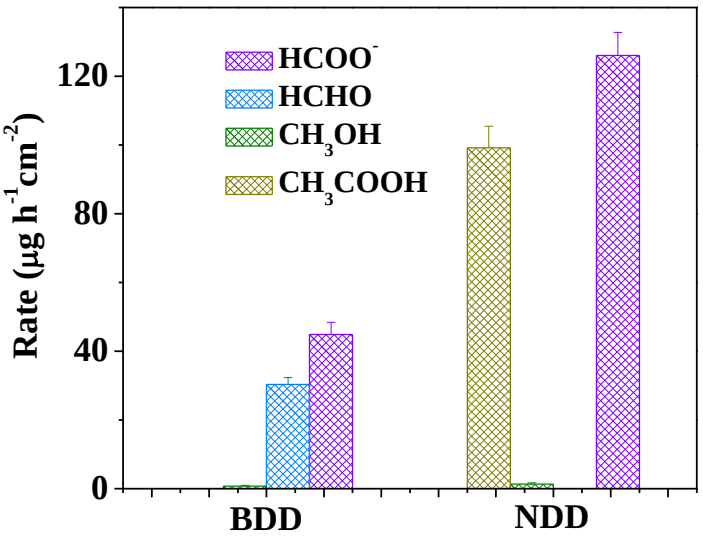

Figure S6. The production rate of products formed during electrochemical reduction of CO_2 on BDD and NDD electrodes.

Figure S7 shows a possible DFT optimized pathway for CO_2 reduction on both (111) and (220) facets proceeds as CO_2 → *COOH → CO* → *COCO. The reaction free energy for converting CO_2 to *COOH has no significant difference on (111) and (220) facets. However, the reaction free energy for *COOH → CO* on (111) facet (1.50 eV) is lower than that on (220) facet (1.79 eV), while the reaction CO* → *COCO is more favorable on (111) facet (reaction free energy -3.32 eV) than (220) facet (reaction free energy -1.76 eV). For the following *COCO reduction reaction, H is easy to transfer to *COCO on (111) facet while it is difficult for H to transfer to *COCO on (220) facet due to that H tends to combine with the surface C atom of (220) facet. These results suggest altered facet may be not the main factor contributed to the superior performance of BND.

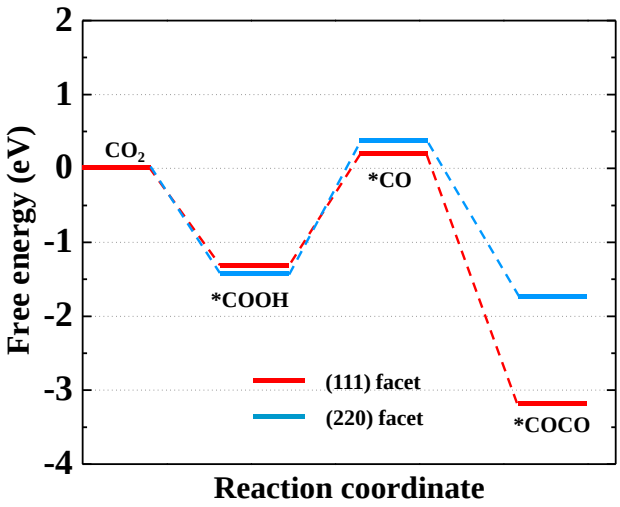

Figure S7. Relative free energy diagrams for CO_2 reduction on (111) and (220) facets of BND.